Simultaneous estimation of soil hydraulic and solute transport parameters from transient infiltration experiments

ARTICLE *in* ADVANCES IN WATER RESOURCES · JUNE 2000

Impact Factor: 3.42 · DOI: 10.1016/S0309-1708(00)00011-7

4 AUTHORS, INCLUDING:

Mitsuhiro Inoue
Tottori University
90 PUBLICATIONS **742** CITATIONS
SEE PROFILE

Jiri, Jirka Simunek
University of California, Riverside
375 PUBLICATIONS **9,447** CITATIONS
SEE PROFILE

Jan W Hopmans
University of California, Davis
320 PUBLICATIONS **6,140** CITATIONS
SEE PROFILE

ELSEVIER

Advances in Water Resources 23 (2000) 677–688

Advances in Water Resources

www.elsevier.com/locate/advwatres

Simultaneous estimation of soil hydraulic and solute transport parameters from transient infiltration experiments

M. Inoue [a], J. Šimůnek [b,*], S. Shiozawa [c], J.W. Hopmans [d]

[a] *Arid Land Research Center, Tottori University, Hamasaka 1390, Tottori 680, Japan*
[b] *US Salinity Laboratory, USDA-ARS, 450 W. Big Springs Dr., Riverside, CA 92507, USA*
[c] *Institute of Agricultural and Forest Engineering, University of Tsukuba, Tsukuba, Japan*
[d] *Hydrology Program, Department LAWR, 123 Veihmeyer Hall, University of California, Davis, CA 95616, USA*

Received 6 October 1999; received in revised form 10 February 2000; accepted 11 February 2000

Abstract

Estimation of soil hydraulic and solute transport parameters is important to provide input parameters for numerical models simulating transient water flow and solute transport in the vadose zone. The Levenberg–Marquardt optimization algorithm in combination with the HYDRUS-1D numerical code was used to inversely estimate unsaturated soil-hydraulic and solute transport parameters from transient matric pressure head, apparent electrical conductivity, and effluent flux measurements. A 30 cm long soil column with an internal diameter of 5 cm was used for infiltration experiments in a coarse-textured soil. Infiltration experiments were carried out with both increasing and decreasing solute concentrations following a sudden increase in the infiltration rate. Matric pressure heads and solute concentrations were measured using automated mini-tensiometers and four-electrode sensors, respectively. The simultaneous estimation results were compared with independently measured soil water retention, unsaturated hydraulic conductivity, and solute dispersion data obtained from steady-state water flow experiments. The optimized values corresponded well with those measured independently within the range of experimental data. The information contained in the apparent electrical conductivity (which integrates information about both water flow and solute transport) proved to be very useful for the simultaneous estimation of soil hydraulic and solute transport parameters.

Keywords: Four-electrode sensor; Bulk soil electrical conductivity; Hydraulic conductivity; Soil water retention curve; Dispersivity

1. Introduction

In arid and semiarid regions that are characterized by high air temperatures and low precipitation rates, salts accumulation at or near the soil surface is common. Soil salinization in irrigated agriculture may be accelerated by the presence of high groundwater table when, for example, deep drainage is reduced because of low subsoil permeability. The combined effects of waterlogging and salinization may cause a significant decrease of agricultural productivity of irrigated lands [17]. When a reliable drainage system is present, salts can be removed from the root zone by leaching using excess irrigation water. Such practices can be conveniently described using models that simulate simultaneously water flow and solute transport processes [22].

Computer models based on numerical solutions of the flow and solute transport equations are increasingly being used for a wide range of applications in soil and water management. Model predictions depend largely on the accuracy of available model input parameters. Soil hydraulic parameters, characterizing the water retention and permeability properties, and transport and chemical parameters affecting the rate of spreading of chemicals and their distribution between solid and liquid phases are the most important input variables for such models.

The use of parameter estimation techniques for determining soil hydraulic properties is well established [2,8]. The approach has been widely used for various laboratory and field experiments. Among others, laboratory experiments include one-step [7,30] and multi-step [1,31] outflow experiments, upward flux or head controlled infiltration [3], the evaporation method

* Corresponding author. Tel.: +1-909-369-4865; fax: +1-909-342-4964.

E-mail addresses: mainoue@center.tottori-u.ac.jp (M. Inoue), jsimunek@ussl.ars.usda.gov (J. Šimůnek), shiozawa@sakura.cc.tsukuba.ac.jp (S. Shiozawa), jwhopmans@ucdavis.edu (J.W. Hopmans).

0309-1708/00/$ - see front matter
PII: S0309-1708(00)00011-7

[20,24], and infiltration followed by redistribution [25]. In separate lines of research, solute transport parameters are often obtained from column experiments assuming steady-state water flow [15], and using parameter estimation codes such as CFITIM [33] or CXTFIT [29] for fitting analytical solutions of the transport equation to experimental breakthrough curves. Solute transport parameters for conditions for which no analytical solutions exist, such as for nonlinear adsorption, can be obtained using numerical solutions [10,25]. The above parameter estimation efforts for water flow and solute transport have remained relatively disjoint. Although there are numerous studies that combined estimation of flow and transport parameters for groundwater flow problems [12,27,34], only a very few studies have used combined transient variably-saturated water flow and solute transport experiments for simultaneous estimation of soil hydraulic and solute transport parameters [13].

Different strategies in combined estimation of water flow and solute transport parameters can be followed. Only water flow information (matric pressure heads and/or fluxes) can be used first to estimate soil hydraulic parameters, followed with estimation of transport parameters using only transport information (concentrations). Combined water flow and transport information can be used to estimate sequentially soil hydraulic and solute transport parameters. Finally, combined water flow and transport information can be used to simultaneously estimate both soil hydraulic and solute transport parameters. The last approach is the most beneficial since it uses crossover effects between state variables and parameters [27] and it takes advantage of the whole information, because concentrations are a function of water flow [12]. Misra and Parker [13] showed that simultaneous estimation of hydraulic and transport properties yields smaller estimation errors for model parameters than sequential inversion of hydraulic properties from water content and matric pressure head data followed by inversion of transport properties from concentration data.

The main motive for the simultaneous estimation of water flow and solute transport parameters in groundwater studies is to use the most information available and to decrease parameter uncertainty. In soil studies, this is accompanied by the motive to avoid carrying out repeated experiments on the same sample. That is, repeated experiments on the same or identically-packed soil columns most likely will affect the magnitude of flow and transport parameters. Moreover, the presented transient flow and transport experiments are more realistic than those requiring steady state. The combined use of transient flow and transport data for estimation of the soil hydraulic and solute transport parameters can also result in substantial time-savings as compared to steady-state methods.

Excellent tools have been developed over the years to analyze transient flow experiments such as ONESTEP [6], SFIT [9], and HYDRUS-1D [23]. Some programs are designed for specific experiments only (e.g., ONESTEP [6]), while others are more versatile (e.g., SFIT [9], HYDRUS-1D [23]). Of the above codes, only HYDRUS-1D allows simultaneous inversion of soil hydraulic and solute transport parameters, including situations involving linear and nonlinear solute transport during either steady-state or transient water flow.

The objective of this study is to determine soil hydraulic and solute transport parameters of a Tottori dune sand using various steady-state and transient water flow and solute transport laboratory column experiments. The transient and steady-state tests involve infiltration at different rates. Parameters determined using different analytical and parameter estimation approaches will be compared. We also discuss the application and calibration of a four-electrode sensor to measure the bulk soil electrical conductivity. The measured bulk soil electrical conductivity is a variable that integrates information on both water flow and solute transport and can thus be beneficially used to estimate simultaneously soil hydraulic and solute transport parameters. We show that the measured bulk soil electrical conductivity is especially advantageous when used for the simultaneous estimation of soil hydraulic and solute transport parameters.

2. Theory

2.1. Water flow

Variably-saturated water flow in porous media is usually described using the Richards equation

$$\frac{\partial\theta(h)}{\partial t}=\frac{\partial}{\partial z}\left(K(h)\frac{\partial h}{\partial z}+K(h)\right), \tag{1}$$

where t is time and z is depth (positive upward), and θ and h denote the volumetric water content and the soil water matric pressure head, respectively. The Richards equation can be solved numerically when the initial and boundary conditions are prescribed and two constitutive relations, i.e., the soil water retention, $\theta(h)$, and hydraulic conductivity, $K(h)$, functions, are specified. The soil water retention curve in this study is described using the van Genuchten analytical expression [32]

$$S_{\mathrm{e}}(h)=\frac{\theta(h)-\theta_{\mathrm{r}}}{\theta_{\mathrm{s}}-\theta_{\mathrm{r}}}=\frac{1}{(1+|\alpha h|^{n})^{m}}. \tag{2}$$

The hydraulic conductivity function is described using the capillary model of Mualem [14] as applied to the van Genuchten function [32]

$$K(h)=K_{\mathrm{s}}S_{\mathrm{e}}^{\ell}\left[1-\left(1-S_{\mathrm{e}}^{1/m}\right)^{m}\right]^{2}. \tag{3}$$

In Eqs. (2) and (3), θ_r and θ_s denote the residual and saturated volumetric water contents, respectively; S_e is effective saturation, K_s the saturated hydraulic conductivity, ℓ a pore connectivity coefficient, and α, n and m $(=1-1/n)$ are empirical coefficients.

2.2. Solute transport

Solute transport in variably-saturated porous media is described using the convection–dispersion equation

$$\frac{\partial R\theta C}{\partial t} = \frac{\partial}{\partial z}\left(\theta D\frac{\partial C}{\partial z}\right) - \frac{\partial v\theta C}{\partial z}, \tag{4}$$

where C is the solute concentration, R the retardation factor, D the effective dispersion coefficient, and v is the pore water velocity. The retardation factor R and the dispersion coefficient D are defined as

$$R = 1 + \frac{\rho_b K_d}{\theta}, \tag{5}$$

$$D = \lambda|v|, \tag{6}$$

where K_d is the linear adsorption distribution coefficient, ρ_b the bulk density, and λ is the longitudinal dispersivity. Eq. (6) assumes that molecular diffusion is insignificant relative to dispersion.

2.3. Initial and boundary conditions

The initial condition for each infiltration experiment was obtained by establishing steady-state downward infiltration with a constant water flux and a constant solute concentration. Then, at some time $t=t_i$, both matric pressure head and solution concentration were constant with depth

$$\begin{aligned} h(z,t_i) &= h_i, \\ C(z,t_i) &= C_i. \end{aligned} \tag{7}$$

The upper boundary conditions ($z=0$) for the infiltration experiments are given by

$$\begin{aligned} -K\left(\frac{\partial h}{\partial z}+1\right) &= q_{top}(t), \\ -\theta D\frac{\partial C}{\partial z} + qC &= q_{top}(t)\,C_{top}(t), \end{aligned} \tag{8}$$

where q_{top} and C_{top} are, respectively, water flux and solute concentration applied at the soil surface.

A zero matric pressure head gradient (free drainage, $q=-K$) and a zero concentration gradient are used as the lower boundary conditions (at $z=-L$) for water flow and solute transport, respectively,

$$\begin{aligned} \left(\frac{\partial h}{\partial z}\right)_{z=-L} &= 0, \\ \left(\frac{\partial C}{\partial z}\right)_{z=-L} &= 0. \end{aligned} \tag{9}$$

The water flow and solute transport equations subject to initial and boundary conditions were solved numerically using the HYDRUS-1D code [23].

2.4. Parameter optimization

The general approach of parameter estimation involves the minimization of a merit, goal or objective function that considers all deviations between the measured and simulated data, with the simulated results controlled by the adjustable parameters to be optimized [26]. The objective function OF($\boldsymbol{b}$) for the transient flow experiments is given by

$$\begin{aligned} \mathrm{OF}(\mathbf{b}) = {} & W_h\sum_{i=1}^{N_1}[h_m(t_i) - h_o(t_i,\mathbf{b})]^2 \\ & + W_q\sum_{i=1}^{N_2}[q_m(t_i) - q_o(t_i,\mathbf{b})]^2, \end{aligned} \tag{10}$$

where W_h, and W_q are normalization factors for matric pressure head and flow rate, respectively, with each factor being inversely proportional to their measurement variance; N_1, and N_2 the number of observations for matric pressure head and flux, respectively; and $\boldsymbol{b}$ is the vector of optimized parameters. The subscripts m and o refer to the measured and optimized values. The weighted least-squares estimator of Eq. (10) is a maximum-likelihood estimator as long as the weights contain the measurement error information of particular measurements.

The objective function for the transport part of the transient experiments is given by

$$\mathrm{OF}(\mathbf{b}) = W_{EC}\sum_{i=1}^{N_3}[EC_{a,m}(t_i) - EC_{a,o}(t_i,\mathbf{b})]^2, \tag{11}$$

where EC_a is the bulk electrical conductivity, W_{EC} its normalization factor, and N_3 is the number of electrical conductivity measurements. The objective function for simultaneous optimization of soil hydraulic and solute transport parameters combines objective functions Eqs. (10) and (11).

The Levenberg–Marquardt method [11,27,34] (as incorporated in the HYDRUS-1D code [23]) was used to minimize the objective function OF($\boldsymbol{b}$). The parameter vector $\boldsymbol{b}$ includes the parameters α, n, θ_r, θ_s, K_s, l, and λ. Each inverse problem was restarted several times with different initial estimates of optimized parameters and the run with the lowest value of the objective function was assumed to represent the global minimum. The soil bulk electrical conductivity, EC_a, was calculated in the HYDRUS-1D code from calculated values of the solution electrical conductivity, EC_w, and the water content, θ (see Section 3.1).

3. Materials and methods

3.1. Electrical conductivity measurements

Nondestructive methods for direct measurement of soil salinity include buried porous electrical conductivity sensors, four-electrode probe systems, electromagnetic induction sensors, and time domain reflectometry systems [16,18]. These methods all measure the bulk soil solute concentration rather than the solution concentration of individual ions [19]. The four-electrode probe is used for measurement of solute concentrations when rapid measurements are needed; this method is well suited for measuring both water flow and solute transport variables simultaneously during transient infiltration and/or evaporation. The main disadvantage of the four-electrode sensor is that soil-specific calibration is required.

The four-electrode sensor developed for this study is described in detail by Shiozawa et al. [21]. The sensor consists of four stainless steel rods of 1 mm outside diameter, which are inserted parallel in the center of an acrylic cylinder ring of 20 mm length and 50 mm inside diameter (Fig. 1). The two inner and two outer stainless steel rods are spaced 8 and 16 mm, respectively.

The ratio of the electric current (I) flowing through the outer electrodes to the voltage difference (V_2) between the two inner electrodes is measured. The ratio I/V_2 is inversely proportional to the electrical resistance of the measured medium, or proportional to its electrical conductivity (EC). The magnitude of the electric current (I) through the two outer electrodes is obtained from $I = V_1/R_f$, where R_f is a known resistance inserted in the circuit (Fig. 1). The ratio V_1/V_2 is automatically measured using a 21X micro-datalogger (Campbell Scientific) which also supplies the required AC of 750 Hz. The proportionality constant between the output value V_1/V_2 and the bulk EC depends on the shape and construction of the sensor, and is determined by measuring known EC-values of various water solutions at a known reference temperature. This was done with all three sensors using sodium chloride solutions in the range between 0.005 and 0.2 mol/l.

The four-electrode sensors were calibrated in mixtures of Tottori dune sand and sodium chloride solutions [4,21]. The measured bulk soil electrical conductivity (EC_a) depends on the electrical conductivity of the soil solution (EC_w), the volumetric water content (θ), the dry bulk density (ρ_b), and temperature of the water solution and the soil (T). After washing the sand with distilled water, clay and silt fractions were removed, and the pure sand samples were oven-dried. Clay and silt fractions were removed in order to prevent potential clogging and permeability changes of the porous plate by transport of these finer fractions during the relatively fast infiltration experiments. Known volumes of NaCl solution with known concentrations were added to the sand to obtain the desired water content and salt concentration values. In all, four-electrode probe calibration was carried out for NaCl concentrations of 0.005, 0.01, 0.02, 0.03, 0.04, 0.05, 0.06, 0.08, 0.1, 0.2, 0.5, and 1.0 mol/l, and for volumetric water content values ranging from 0.0287 to 0.454 cm^3/cm^3, including full saturation. The mixtures were kept in a vinyl bag at a constant temperature of 25°C for two days. A total of 96 prepared soil samples were packed uniformly in columns of 50 mm inside diameter and 60 mm height, and the surfaces leveled and covered to prevent evaporation. After measurement of EC_a with the four-electrode sensor, the volumetric water content and the dry bulk density of each soil sample were determined from oven-drying. The average value of the dry bulk density (ρ_b) was 1.45 ± 0.02 g/cm^3 at an average soil temperature of $T = 25.0 \pm 0.5$°C.

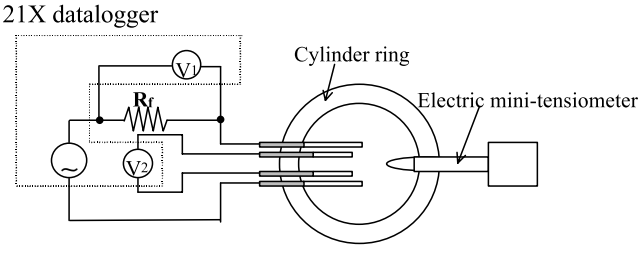

Fig. 1. The four-electrode sensor and the electric circuit.

We assumed that the relation between EC_a and EC_w can be described by the following relationship, which neglects the surface conductance of the solid phase [17]

$$\frac{EC_a}{\theta} = a(EC_w \cdot \theta) + b. \tag{12}$$

The surface conductance, associated with the exchangeable ions at the solid–liquid interface, can be neglected only for sandy soil. Rhoades and Oster [18] discussed relations between EC_a and EC_w for situations when the surface conductance cannot be neglected, such as for silt and clay fractions. The fitted relations of EC_a versus θ are shown in Fig. 2 for various solution concentrations; symbols in the figure are experimental values and the lines represent the fitted Eq. (12). Fitted values for a and b were 1.45 and 0.102, respectively, with a correlation coefficient value of 0.998.

To convert EC_w to concentration, the following experimentally derived power relationship was used [4]

$$C = 0.008465 \cdot EC_w^{1.073}. \tag{13}$$

Using Eq. (12), the water content can be determined if the pore water salinity, EC_w, is known, or alternatively EC_w can be computed from the measured EC_a and a known θ. Average relative errors were calculated using the expression $100 \sum(|Y_m - Y_e|/Y_e)/n$, where n, Y_e and Y_m represent the number of experimental data, and

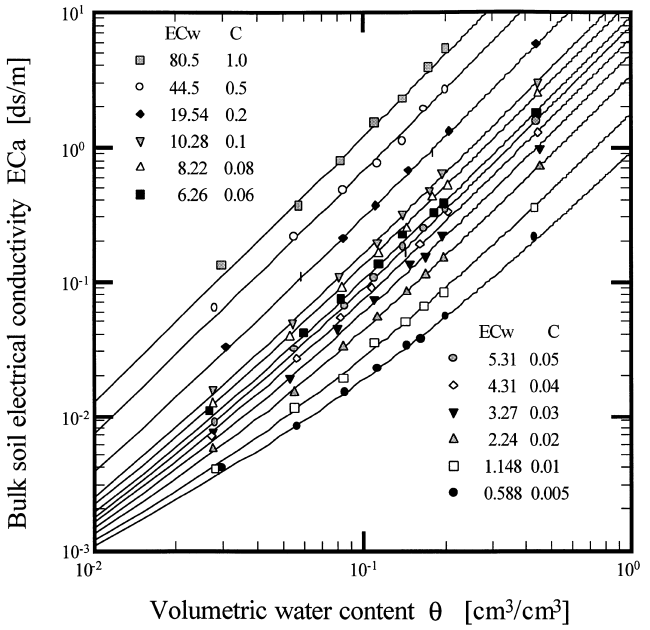

Fig. 2. Calibration of the four-electrode sensor for dune sand. Lines represent fitted Eq. (2) for different concentrations (different electrical conductivities of the soil solution as given in the legend), with the highest concentration at the top and lowest at the bottom.

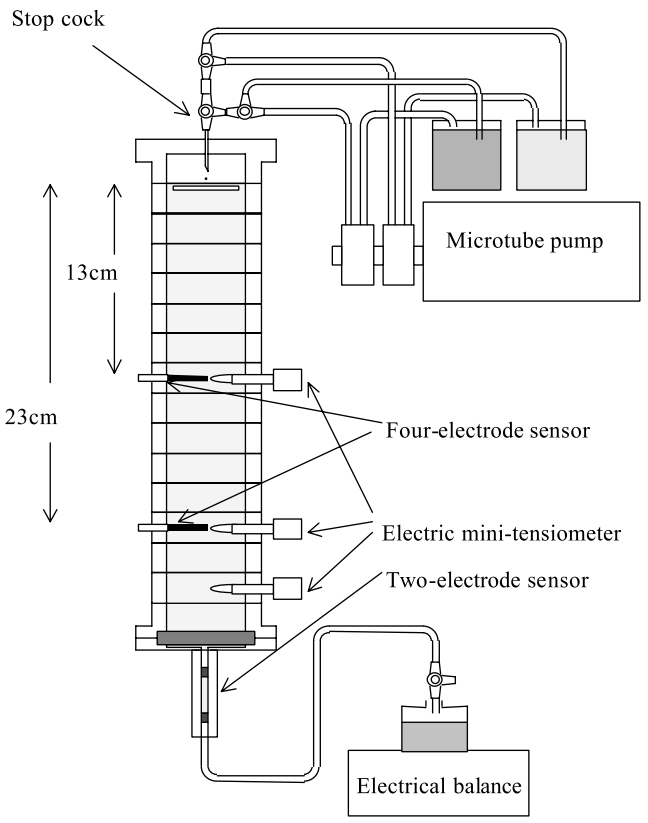

Fig. 3. Schematic illustration of the column experimental setup.

estimated and experimental values, respectively. We obtained average errors of 2.41% and 5.60% for the volumetric water content and the soil water electrical conductivity, respectively. Hence, the four-electrode probe can be conveniently used to measure either water content θ or concentration C.

3.2. Steady-state infiltration experiments

Four-electrode probes and mini-tensiometers were used to determine the soil water retention curve from steady-state downward infiltration into the washed Tottori sand. The experimental setup consisted of a soil column of 50 mm diameter and 30 cm height, and a balance to measure the drainage rate (Fig. 3) [34]. The soil column was packed under wet condition at the bulk density of 1.50 ± 0.03 g/cm^3. Two mini-tensiometers with pressure transducers and four-electrode sensors were installed at the 13 and 23 cm depths, and an additional tensiometer at the 27 cm depth. A 5 mm thick coarse-sintered glass plate with a saturated conductivity value of 0.000405 cm/s was placed at the bottom.

Using the syringe pump a constant infiltration rate of a NaCl solution having a constant concentration of 0.02 mol/l was applied to the soil surface. After establishing a steady drainage rate at saturation, the infiltration rate was first decreased in steps (to obtain drying retention data) and then increased (providing wetting retention data). Variations in the soil water matric pressure head (h) and the bulk electrical conductivity (EC_a) with time were measured using the mini-tensiometers and the four-electrode sensors, respectively. The matric pressure head at the bottom of the column was continuously adjusted to the value monitored by mini-tensiometer at the 23 cm depth. Since the solution concentration (C) was known and constant, EC_w was determined directly from Eq. (13). Hence, the water content, θ, could be estimated directly using Eq. (12) and the four-electrode sensor's measurement of EC_a.

We then conducted a series of eight steady-state flow experiments with steady-state infiltration fluxes (i) varying between 0.022 and 0.00036 cm/s (first column of Table 1). Using the steady-state data of the four-electrode sensors and mini-tensiometers at column depths of 13 and 23 cm, unsaturated hydraulic conductivities, K, were calculated with Darcy's law from the known steady-state water fluxes and measured total hydraulic head gradients, dH/dz. Since flow is steady state, the water flux is equal to the infiltration rate at any column depth. The results in Table 1 show that the hydraulic gradient dH/dz is near unity during each of the experiments, and that unsaturated hydraulic conductivity K is a rapidly decreasing function of θ. The values of v, θ, h, K, and dH/dz, presented in Table 1 are average values between depths of 13 and 23 cm.

Once steady-state water flow was established over the entire soil column, the NaCl concentration of the inflow

Table 1
Estimation of unsaturated hydraulic conductivities, dispersivities, and dispersion coefficients from steady-state water flow experiments[a]

i (cm/s)	v (cm/s)	θ (cm^3/cm^3)	h (cm)	dH/dz (cm/cm)	K (cm/s)	λ (cm)	D (cm^2/s)
0.0219	0.0727	0.301	−11.9	1.036	0.0211	0.157	0.0114
0.0185	0.0668	0.277	−11.2	1.063	0.0174	0.162	0.0108
0.0151	0.0583	0.259	−12.6	0.928	0.0163	0.232	0.0135
0.00869	0.0382	0.227	−13.7	1.008	0.00862	0.304	0.0116
0.00506	0.0249	0.203	−12.4	0.968	0.00522	0.280	0.0070
0.00227	0.0134	0.169	−14.1	1.004	0.00226	0.278	0.0037
0.00105	0.0075	0.140	−15.5	0.945	0.00111	0.272	0.0020
0.00036	0.0030	0.121	−18.0	1.020	0.00035	0.190	0.00056

[a] i – Infiltration rate, v – pore water velocity, θ – volumetric water content, h – matric pressure head, dH/dz – total head gradient, K – hydraulic conductivity, λ – dispersivity, D – dispersion coefficient.

solution was changed from 0.02 to 0.1 mol/l. The EC in the soil column was measured at two depths using the four-electrode sensors, while the EC of the effluent was measured with a two-electrode sensor in the outflow tube at the bottom of the soil column (Fig. 3). As an example, we present here the experimental results for a steady-state water flux of $i = 0.00506$ cm/s, corresponding to a soil water matric pressure head h of −12.4 cm, a mean pore water velocity v of 0.0249 cm/s, and an average volumetric water content θ of 0.203 cm^3/cm^3. The breakthrough curves using relative concentration for the three depths of 13, 23, and 30 cm are shown in Fig. 4. Dispersion coefficient, D, dispersivity values, λ, and mean pore water velocity, v, were determined by fitting the analytical solution of the convection–dispersion equation to the measured concentration values using the CXTFIT program [31]. The average volumetric water content, θ, was then calculated from a steady-state water flux, i, and a mean pore water velocity, v ($\theta = i/v$). Dispersivity values estimated from each of the eight steady-state experiments for the breakthrough curves measured at the 23 cm depth are presented in Table 1. Similar dispersivity values, as those give in Table 1, were obtained when we analyzed breakthrough curves at depths of 13 and 30 cm. Although pore water velocities varied more than one order of magnitude (0.0030–0.0727 cm/s), dispersivity values were reasonably close (0.157–0.304 cm). The dispersivities were computed using Eq. (6) from the estimated pore water velocities and fitted dispersion coefficients.

3.3. Transient infiltration experiments

The scanning wetting and drying water retention curves were obtained by matching matric pressure head and water content values measured during the transient infiltration experiments. From the simultaneous measurements at the 23 cm depth during three wetting (applied flux varying between 0.4 and 3.2 ml/min) and two drying (flux varying between 3.2 and 0.4 ml/min) processes, the hysteretic relationships between θ and h could be determined as shown in Fig. 5.

We subsequently conducted three infiltration experiments (Experiment I, II, and III) to simultaneously measure the hydraulic and solute transport variables. In each of the three experiments, the initial steady-state

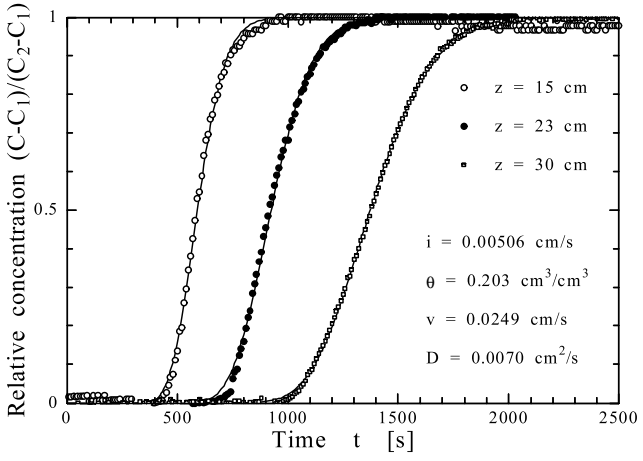

Fig. 4. Breakthrough curves of NaCl solution measured using four-electrode (at depths of 13 and 23 cm) and two-electrode (at a depth of 30 cm) sensors in the unsaturated sand column and fitted using the CXTFIT code.

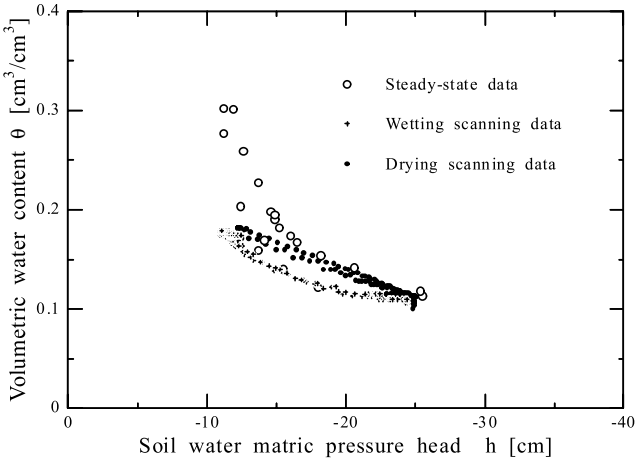

Fig. 5. Wetting and drying soil water retention curves obtained using measurements of mini-tensiometer and four-electrode sensor at a depth of 23 cm during steady-state and transient infiltration experiments.

Table 2
Summary of transient infiltration experiments

Experiment no.	I (cm/s)	C (mol/l)	h_{2i} (cm)	Measured variables
I	$i_i = 0.00033$ $i_f = 0.00278$	$C_i = 0.02$ $C_f = 0.1$	−24.7	h_1, h_2, h_3, q, EC_{a1}, EC_{a2}
II	$i_i = 0.000321$ $i_f = 0.002581$	$C_i = 0.02$ $C_f = 0.1$	−26.8	h_2, EC_{a2}
III	$i_i = 0.000312$ $i_f = 0.002632$	$C_i = 0.1$ $C_f = 0.02$	−27.2	h_2, EC_{a2}

infiltration rate (i) of about 0.00032 cm/s was increased to about 0.0026 cm/s at time $t = 1000$ s. For Experiments I and II, the solute concentration, C, was increased from 0.02 to 0.1 mol/l simultaneously with the infiltration rate increase. The solute concentration was decreased from 0.1 to 0.02 mol/l at $t = 1000$ s in Experiment III. Table 2 summarizes the applied infiltration rates and solute concentrations, combined with the type of measurements, and at which depth they were taken. Subscripts 1, 2, and 3 refer to depths of 13, 23, and 27 cm, respectively, and the subscripts i and f denote the initial and final stages of the infiltration experiment, respectively.

4. Results and discussion

4.1. Experimental data

Observed values of h, EC_a, and calculated values of θ and C versus time at the 23 cm depth for Experiment II are shown in Fig. 6. The values of h and EC_a were directly measured with the mini-tensiometer and the four-electrode sensor, respectively. The values of in θ with time were computed from the measured h values, while those of C were calculated from the measured EC_a and the estimated θ using Eqs. (12) and (13). As shown in Fig. 6, the water content θ and the solution concentration C at the 23 cm depth started increasing at about 1250 and 2400 s, respectively. Hence, the concentration front lags behind the moisture front. This observation is well known and occurs because new infiltrating water displaces old water initially present in the porous media, and because of diffusion, mixing and equilibration of solute between the new and old water. The old water with the initial solute concentration is thus pushed in front of the advancing new water with the new solute concentration. This process results into separate water and solute fronts, each traveling at different speeds depending on the ratio of the initial and final water contents [5,28]. The higher infiltration rate during the second stage increased h_2 from −26 to about −13, corresponding to an increase in θ from 0.12 cm^3/cm^3 to 0.19 cm^3/cm^3. The EC_a curve in Fig. 6 also clearly shows the combined control of both water content and solution concentration on the bulk electrical conductivity curve. This combined effect of θ and C on EC_a results in two fronts, the first one at about 1250 s caused by wetting front, and the second one starting at about 2500 s responding to the concentration front.

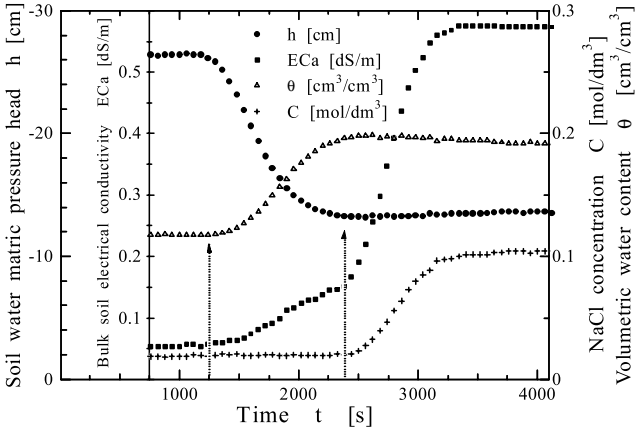

Fig. 6. Variation of h, EC_a, θ, C with time at a depth of 23 cm in the soil column after changing both q (from 0.000321 to 0.00258 cm/s) and C (0.02 to 0.1 mol/dm^3) at $t = 1000$ s (Experiment II).

The results of Experiment III for the 23 cm depth are presented in Fig. 7. As the water content increased because of the higher infiltration rate, the bulk electrical conductivity, EC_a, increased during the time interval between 1250 and 2300 s. However, the decreasing solute concentration at about 2300 s caused the EC_a to decrease after that time. As in Experiments I and II, the initial part of the EC_a curve reflects mainly changes in θ, whereas the second part of the curve characterizes solute transport properties.

4.2. Inverse analysis

4.2.1. Hydraulic parameters

We next used the parameter optimization features if HYDRUS-1D to analyze the θ and C distributions. To better understand the possible influence of the porous plate at the bottom of the column, we compared optimization results for profiles with a plate (using a two-

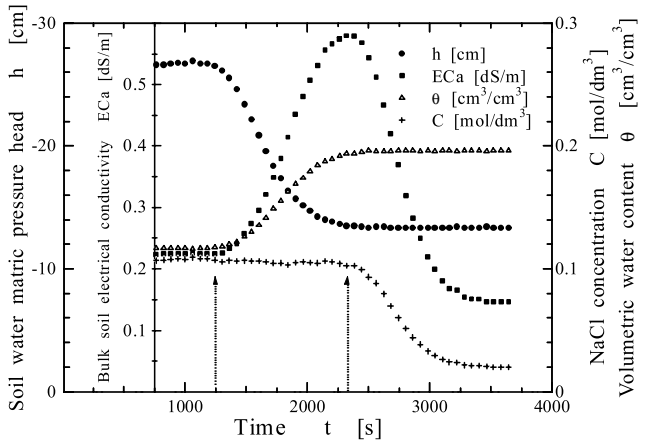

Fig. 7. Variation of h, EC_a, θ, C with time at a depth of 23 cm in the soil column after changing both q (from 0.000312 to 0.00263 cm/s) and C (0.1 to 0.02 mol/dm^3) at $t = 1000$ s (Experiment III).

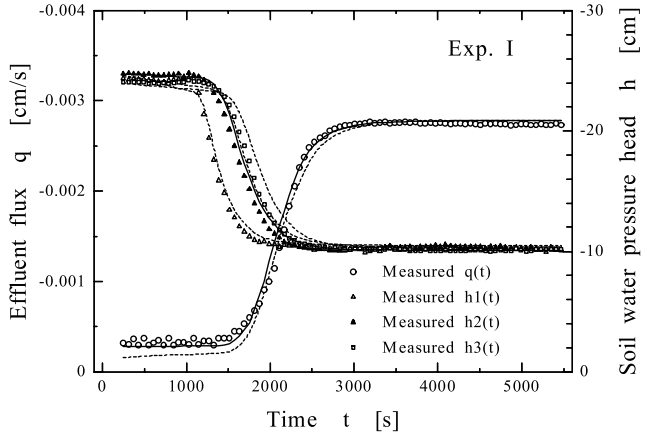

Fig. 8. Measured and optimized outflow rates and matric pressure heads for Experiment I. Either a one-layer (solid lines) or two-layer (dashed lines) models were used in the inverse analysis.

layer model) and without a plate (using a one-layer model). The columns for this purpose were first schematized as a two-layered profile with the Tottori sand representing the first layer and the sintered glass plate representing the second layer. The saturated hydraulic conductivity of the plate was independently measured and found equal to 0.000405 cm/s. Fig. 8 shows the measured and optimized flow rates, $q(t)$, and the matric pressure heads $h_1(t)$, $h_2(t)$, $h_3(t)$ for depths of 13, 23, and 27 cm of Experiment I. Results reveal a very good agreement between the measured and optimized values of both the outflow rate (q) and matric pressure head (h). Only the arrival of the water content front to tensiometer at depth of 27 cm lags behind the model prediction. The inversely obtained parameters are listed in Table 3 (first row).

Optimized flow rates and matric pressure head values for the 23 cm depth of Experiment I using the one-layer model and the free drainage bottom boundary condition are also shown in Fig. 8. The correspondence between measured and optimized values for both outflow rates and matric pressure heads are similar to those when a two-layer model was used. The optimized parameters obtained with the one-layer model for Experiment I are also listed in Table 3 (second row). The optimized parameters are also very similar with those obtained using the two-layer model and 95% confidence intervals for all optimized parameters overlapped. Only the l parameter differs by about one-third between the two solutions, but that has no significant consequence on the prediction of the hydraulic conductivity function within the measurement range (Fig. 9). Fig. 9 compares the optimized soil water retention and hydraulic conductivity functions for both the one-layer and two-layer models, and independent data obtained using the steady-state and transient infiltration methods. Notice that all optimized functions closely approximate the independently measured data within the water content range of the transient experiments ($0.1 < \theta < 0.2$) and that larger differences exist only beyond the measurement range. Since results for two- and one-layered systems were similar, we conclude that the sintered glass plate did not significantly influence flow at the measurement depths (13 and 23 cm) used in optimization calculations.

4.2.2. Transport parameters

Next, we optimized solute transport parameters for Experiment I using the objective function of Eq. (11), and fixing the already optimized soil hydraulic parameters for water flow. The measured and optimized bulk

Table 3
Optimization results for transient flow and transport experiments

Experiment	Optimized parameter values						
	θ_r (cm^3/cm^3)	θ_s (cm^3/cm^3)	α (cm^{-1})	n	K_s (cm/s)	l	λ (cm)
I (two-layer)	0.0	0.385	0.163	2.05	0.090	−0.66	
I (one-layer)	0.0	0.345	0.164	1.89	0.070	−1.05	
I (two-layer)							0.243
I (one-layer)							0.246
II (one-layer)	0.027	0.310	0.138	2.01	0.045	−1.16	0.221
III (one-layer)	0.057	0.372	0.117	2.42	0.0514	−0.813	0.190

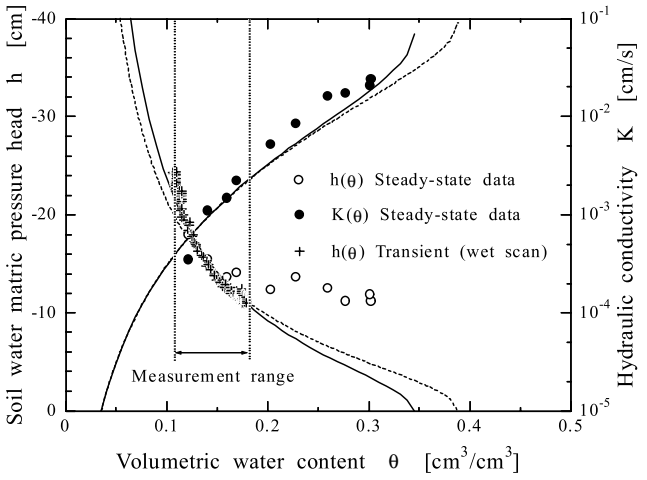

Fig. 9. Comparison between soil hydraulic properties estimated inversely for Experiment I using either a one- (solid lines) or two-layer (dashed lines) models and those obtained from analysis of steady-state and transient infiltration data.

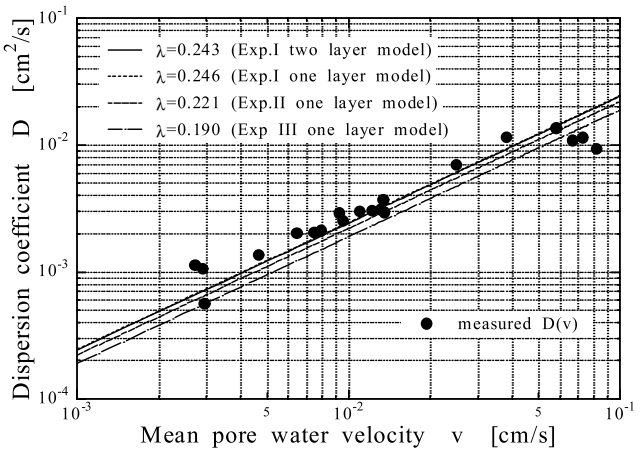

Fig. 11. The dispersion coefficient D as function of the mean pore water velocity v obtained by inverse optimization and from analysis of steady-state data.

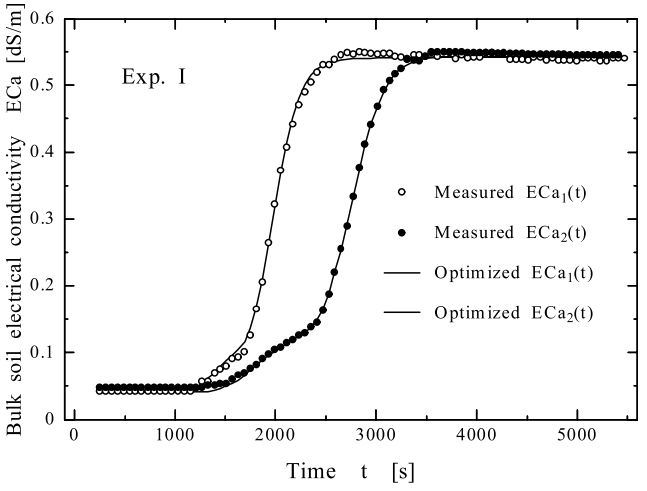

Fig. 10. Measured and optimized bulk electrical conductivities for Experiment I. A one-layer model was used in the inverse analysis.

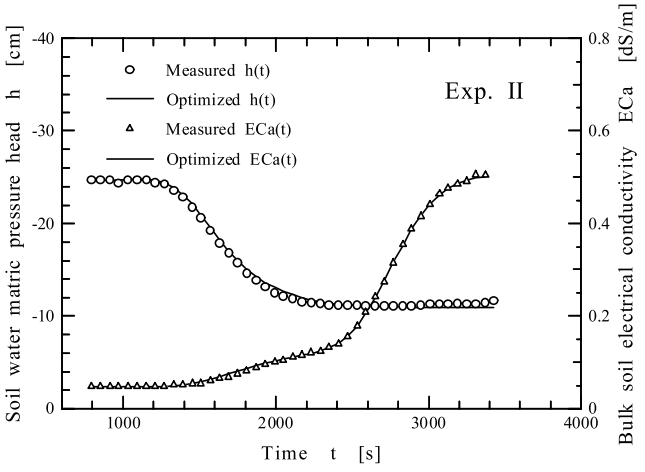

Fig. 12. Measured and optimized matric pressure heads and bulk electrical conductivities for Experiment II. A one-layer model was used in the inverse analysis.

soil electrical conductivities, $EC_{a1}(t)$ and $EC_{a2}(t)$, at depths of 13 and 23 cm, respectively, are presented in Fig. 10. As discussed above, the initial small increase of the bulk soil electrical conductivity corresponds with the arrival of the moisture front, whereas the second, steeper and larger increase corresponds with the concentration front. Excellent agreement was obtained between the measured and optimized EC_a-values. The optimized dispersivities λ were equal to 0.246 and 0.243 cm using a one- and two-layer models, respectively. This shows that the porous plate also did not significantly affect the dispersivity. Fig. 11 compares the optimized dispersion coefficients with the independently measured values obtained with the steady-state column experiments (Table 1). Again, notice the excellent agreement between dispersion coefficients obtained from transient and steady-state experiments.

4.2.3. Simultaneous optimization of hydraulic and transport parameters

The next case involves transient Experiment II, again with an increasing infiltration flux and increasing solute concentration, for which hydraulic and solute transport parameters were optimized simultaneously using the one-layer model. The optimized and measured matric pressure heads and bulk soil electrical conductivities for the 23 cm depth are presented in Fig. 12. As indicated earlier, this figure also clearly shows that the positions of the wetting and solute fronts are distinct, with their positions being a function of the initial water content.

Since the initial (θ_i) and final (θ_f) water contents were about 0.12 and 0.19, and the initial (i_i) and final (i_f) infiltration rates about 0.00032 and 0.00258, respectively, one may expect the wetting front (f_w) to move about 2.7 times faster than the concentration front (f_s):

$$f_w = \left[\frac{i_f - i_i}{i_f} \cdot \frac{\theta_f}{\theta_f - \theta_i}\right] f_s. \quad (14)$$

This means that the center of the concentration front should arrive approximately 2.7 times later than the wetting front at some location in the column. The measured centers of the wetting and concentration fronts (defined here as the arithmetic averages of the initial and final values of the matric pressure head and the concentration, respectively) reached the 23 cm depth at 640 and 1780 s after the change in the infiltration rate, respectively. Thus, the concentration front arrived about 2.78 times later than the wetting front, which agrees well with the estimated value of 2.7, according to Eq. (14). Therefore, information contained in the two fronts does not overlap and can be used to advantage for the simultaneous estimation of soil hydraulic and solute transport parameters. Fig. 13 compares the inversely estimated hydraulic functions against the independently measured data. Notice again the excellent correspondence of the optimized retention curve and the transient wetting data within the experimental range. Optimization results are also presented in Table 3.

Finally, we optimized simultaneously the hydraulic and solute transport parameters to data from Experiment III, i.e., the experiment in which the infiltration rate was increased (from 0.000312 to 0.00263 cm/s) and the solute concentration decreased (from 0.1 to 0.02 mol/l) at $t = 1000$ s. The comparison of measured and simulated h and EC data at the 23 cm column depth is shown in Fig. 14. Again, excellent agreement exists between the optimized and measured soil water matric pressure heads, $h(t)$, and bulk soil electrical conductivities, $EC_a(t)$. Similarly as for Experiment II, the water front moved about 2.7 times faster than the concentration front. The optimized soil hydraulic functions are compared in Fig. 13 with optimization results based on Experiment II, and with the independently measured retention and hydraulic conductivity data. While there is a very good correspondence between the hydraulic conductivities obtained from the different experiments, the optimized retention curve for Experiment III is slightly shifted towards higher water contents as compared with the curve for Experiment II. The parameter estimates are again presented in Table 3. The optimized dispersivity value, however, compares again very well with the independently measured values and with the optimized values from the other infiltration experiments (Fig. 11).

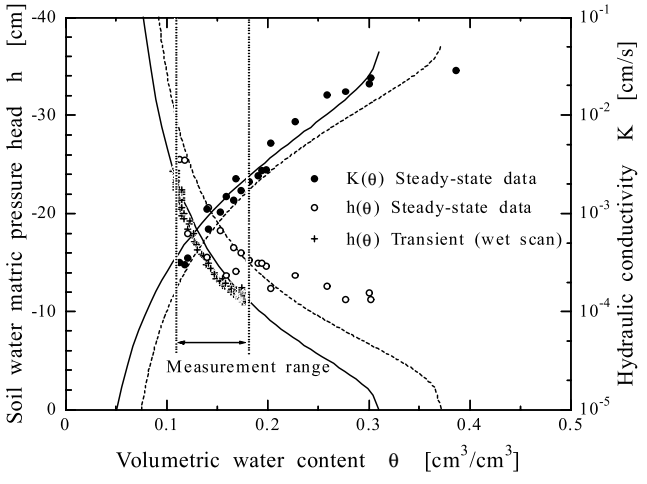

Fig. 13. Comparison between soil hydraulic properties estimated inversely for Experiments II (solid lines) and III (dashed lines) using a one-layer model and obtained from analysis of steady-state and transient infiltration data (data points).

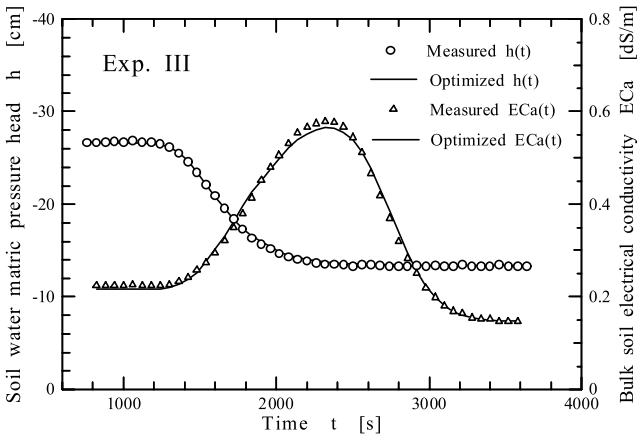

Fig. 14. Measured and optimized matric pressure heads and bulk electrical conductivities for Experiment III. A one-layer model was used in the inverse analysis.

5. Summary and conclusions

Matric pressure head and solute concentration were simultaneously measured during infiltration of sodium chloride solution using mini-tensiometers with pressure transducers and four-electrode sensors. Both the tensiometers and four-electrode sensors proved to be useful for measuring the rapid changes in matric pressure head and electrical conductivity during the simultaneous movement of water and solute in the sandy soil columns. The bulk soil electrical conductivity (EC_a) depends on the solution electrical conductivity (EC_w) and the volumetric water content (θ). After calibrating the functional relation of $EC_a = f(EC_w, \theta)$ for each soil, EC_w can be obtained from the measured EC_a and the known θ.

Alternatively, θ can be obtained from the measured EC_a and a known EC_w. In either case, EC_a can be measured accurately using the calibrated four-electrode sensor. The more complex functional relation would be needed for finer textured soils [18].

The Levenberg–Marquardt algorithm [11] in combination with the HYDRUS-1D (version 2.0) [23] code was used to inversely estimate the unsaturated soil hydraulic and solute transport parameters from transient matric pressure head, soil bulk electrical conductivity and flux measurements. Experiments were carried out with both increasing and decreasing solute concentrations following a sudden increase in the infiltration rate in a sand-filled column. Optimization results were compared with independently measured soil water retention, unsaturated hydraulic conductivity and solute dispersion data. The optimized values corresponded well with those measured independently within the experimental range. Larger differences between fitted functions existed only outside the measurement range. However, it is generally accepted that parameters obtained with parameter estimation are to be used only within the measurement range for which they were determined [24].

Since the apparent electrical conductivity, EC_a, integrates information about both water flow and solute transport, information imbedded in EC_a proved to be very useful for the simultaneous estimation of the soil hydraulic and solute transport parameters. Infiltration experiments produced two distinctive fronts for water movement and solute transport, and thus the effects of water content and concentration changes could be well distinguished. Application of the parameter estimation technique, which combines a numerical solution of the governing partial differential equations with the Levenberg–Marquardt method, to transient water flow and solute transport data resulted in accurate estimation of the soil hydraulic and solute transport parameters. The combined use of transient flow and transport data for estimation of the soil hydraulic and solute transport parameters resulted in substantial timesaving as compared to steady-state methods. The presented method with simultaneous measurement of water flow and solute transport variables using a four-electrode probe and coupled estimation of soil hydraulic and solute transport parameters can be a very efficient method for multi-dimensional field experiments as well.

References

[1] Eching SO, Hopmans JW, Wendroth O. Unsaturated hydraulic conductivity from transient multi-step outflow and soil water pressure data. Soil Sci Soc Am J 1994;58:687–95.

[2] Hopmans JW, Šimunek J. Review of inverse estimation of soil hydraulic properties. In: van Genuchten MTh, Leij FJ, Wu L, editors. Characterization and measurement of the hydraulic properties of unsaturated porous media. University of California, Riverside, CA, 1999, p. 643–59.

[3] Hudson DB, Wierenga PJ, Hills RG. Unsaturated hydraulic properties from upward flow into soil cores. Soil Sci Soc Am J 1996;60:388–96.

[4] Inoue M. Simultaneous movement of salt and water in an unsaturated sand column. ALRC's Annual Report 1993–94, Arid Land Research Center, Tottori University, 1994. p. 1–26.

[5] Kirda C, Nielsen DR, Biggar JW. Simultaneous transport of chloride and water during infiltration. Soil Sci Soc Am Proc 1973;37(3):339–45.

[6] Kool JB, Parker JC, van Genuchten MTh. ONESTEP: A nonlinear parameter estimation program for evaluating soil hydraulic properties from one-step outflow experiments. Virginia Agric Exp Stat Bull 1985;85(3).

[7] Kool JB, Parker JC, van Genuchten MTh. Determining soil hydraulic properties from one-step outflow experiments by parameter estimation: I. Theory and numerical studies. Soil Sci Soc Am J 1985b;49:1348–54.

[8] Kool JB, Parker JC, van Genuchten MTh. Parameter estimation for unsaturated flow and transport models – a review. J Hydrol 1987;91:255–93.

[9] Kool JB, Parker JC. Estimating soil hydraulic properties from transient flow experiments: SFIT user's guide. Electric Power Research Institute Report, Palo Alto, CA, 1987.

[10] Kool JB, Parker JC, Zelazny LW. On the estimation of cation exchange parameters from column displacement experiments. Soil Sci Soc Am J 1989;53:1347–55.

[11] Marquardt DW. An algorithm for least-squares estimation of nonlinear parameters. SIAM J Appl Math 1963;11:431–41.

[12] Medina A, Carrera J. Coupled estimation of flow and solute transport parameters. Water Resour Res 1996;32(10):3063–76.

[13] Mishra S, Parker JC. Parameter estimation for coupled unsaturated flow and transport. Water Resour Res 1989;25(3):385–96.

[14] Mualem Y. A new model for predicting the hydraulic conductivity of unsaturated porous media. Water Resour Res 1976;12:513–22.

[15] Nkedi-Kizza P, Biggar JW, Selim HM, van Genuchten MTh, Wierenga PJ, Davidson JM, Nielsen DR. On the equivalence of two conceptual models for describing ion exchange during transport through an aggregated oxisol. Water Resour Res 1984;20:1123–30.

[16] Rhoades JD. Instrumental field methods of salinity appraisal. In: Topp GC, Reynolds WD, Green RE, editors. Advances in measurement of soil physical properties: bringing theory into practice. SSSA Special Pub. No. 30, 1992. p. 231–48.

[17] Rhoades JD. Sustainability of irrigation: an overview of salinity problems and control strategies. CWRA 1997 Annual Conference Footprints of Humanity: Reflections on 50 Years of Water Resource Developments, Lethbridge, Alberta, Canada, 3–6 June 1997. p. 1–42.

[18] Rhoades JD, Oster JD. Solute content, In: Klute A, editor. Method of soil analysis part 1. 2nd ed. SSSA, Madison, WI, 1986. p. 985–94.

[19] Robbins CW. Field and laboratory measurements. In: Tanji KK, editor. Agricultural salinity assessment and management. ASCE Manuals and Reports on Engineering Practice No. 71, 1990. p. 201–04.

[20] Santini A, Romano N, Ciollaro G, Comegna V. Evaluation of a laboratory inverse method for determining unsaturated hydraulic properties of a soil under different tillage practices. Soil Sci 1995;160:340–51.

[21] Shiozawa S, Inoue M, Toride N. Solute transport under unsaturated unit gradient water flow monitored in soil columns. Soil Sci Soc Am J, submitted.

[22] Šimůnek J, Suarez DL. Sodic soil reclamation using multicomponent transport modeling. ASCE J Irrig Drain Eng 1997;123(5):367–76.
[23] Šimůnek J, Šejna M, van Genuchten MTh. The HYDRUS-1D software package for simulating water flow and solute transport in two-dimensional variably saturated media. Version 2.0, IGWMC – TPS – 70, International Ground Water Modeling Center, Colorado School of Mines, Golden, CO, 1998.
[24] Šimůnek J, Wendroth O, van Genuchten MT. A parameter estimation analysis of the evaporation method for determining soil hydraulic properties. Soil Sci Soc Am J 1998b;62(4):894–905.
[25] Šimůnek J, van Genuchten MTh. Using the HYDRUS-1D and HYDRUS-2D codes for estimating unsaturated soil hydraulic and solute transport parameters. In: vanGenuchten MTh, Leij FJ, Wu L, editors. Characterization and measurement of the hydraulic properties of unsaturated porous media. University of California, Riverside, CA, 1999. p. 1523–36.
[26] Šimůnek J, Hopmans JW. Parameter optimization and nonlinear fitting. In: Dane JH, Topp GC, editors. Methods of soil analysis, part 1. physical methods. 3rd ed. SSSA, Madison, WI, 2000.
[27] Sun N-Z, Yeh WW-G. Coupled inverse problems in groundwater modeling. 1. Sensitivity analysis and parameter identiification. Water Resour Res 1990;26(10):2507–25.
[28] Smiles DE, Philip JR, Knight JH, Elrick DE. Hydrodynamic dispersion during absorption of water by soil. Soil Sci Soc Am J 1978;42:229–34.
[29] Toride N, Leij FJ, vanGenuchten MTh. The CXTFIT code for estimating transport parameters from laboratory or field tracer experiments. Version 2.0, Research Report No. 137, US Salinity Laboratory, USDA, ARS, Riverside, CA, 1995.
[30] van Dam JC, Stricker JNM, Droogers P. Inverse method for determining soil hydraulic functions from one-step outflow experiment. Soil Sci Soc Am J 1992;56:1042–50.
[31] van Dam JC, Stricker JNM, Droogers P. Inverse method to determine soil hydraulic functions from multistep outflow experiment. Soil Sci Soc Am J 1994;58:647–52.
[32] van Genuchten MTh. A closed-form equation for predicting the hydraulic conductivity of unsaturated soils. Soil Sci Soc Am J 1980;44:892–8.
[33] van Genuchten MTh. Non-equilibrium transport parameters from miscible displacement experiments. Research Report No. 119, US Salinity Laboratory, USDA, ARS, Riverside, CA, 1981.
[34] Weiss R, Smith L. Parameter space methods in joint parameter estimation for groundwater flow models. Water Resour Res 1998;34(4):647–61.